



Structure Investigation of Solid Ion Pairs of Three Azole Drugs-rose Bengal Using Different Spectroscopic Techniques and their Biological Activities



Mohamed A. Zayed*¹ and Marwa A. Abdallah²

¹Chemistry Department, Faculty of Science, Cairo University, Giza-12613, Egypt.

²National Organization for Drug Control and Research (NODCAR), Giza, Egypt.

THE present work is concerned with preparation, separation and structure elucidation of solid ion-pairs of three antifungal drugs Fluconazole (FLZ), Voriconazole (VRZ) and Butoconazole nitrate (BTZ) with Rose Bengal (Rbeng). The solid ion-pairs were prepared and investigated using FT-IR, mass spectral (MS) and thermal analyses (TA), in addition to elemental analysis (EA). The general formulae of the prepared ion-pairs were determined. Moreover, the formulae of prepared ion-pairs were proposed and structurally identified. The biological activities of the separated solid ion-pairs towards five types of bacteria and one type fungi in comparison with their drugs were studied, and they were found to be biologically active more than their parent drugs.

Keywords: Voriconazole, Fluconazole, Butoconazole nitrate, Rose Bengal, Ion pairs, Infrared spectra, Thermal analysis, mass spectrometry, Biological activities.

Introduction

Azole antifungals are widely used for the treatment of superficial and invasive fungal infection. Also they are classified as imidazoles or triazoles on the basis of whether they have two or three nitrogen in the five-membered azole ring [1]. Azole antifungal agents prevent the synthesis of ergosterol, a major component of fungal plasma membranes, by competitively inhibiting the cytochrome P450-dependent enzyme lanosterol 14 α -demethylase ((P45014DM, CYP51) [2-5]. Voriconazole, designated chemically as (2R, 3S)-2-(2, 4-difluorophenyl)-3-(5-fluoro-4-pyrimidinyl)-1-(1H-1, 2, 4-triazole-1-yl)-2-butanol (II), is currently the drug of choice for the treatment of invasive aspergillosis [2]. Fluconazole, [2-(2, 4-difluorophenyl)-1, 3-bis (1H-1, 2, 4-triazol-1-yl) propan-2-ol] (I), is an orally active antifungal agent, which is used in the treatment of superficial and systemic candidiasis and Cryptococci infections in patients with the acquired immunodeficiency syndromes (AIDS) [7]. Voriconazole and Fluconazole are

triazole antifungals. Butoconazole nitrate, [(\pm)-1-[4-(p-Chlorophenyl)-2-[2,6-dichlorophenyl) thiol] butyl]-1H-imidazole mononitrate] (III), is an imidazole antifungal; which is primarily used for the local treatment of vulvovaginal candidiasis (infections caused by Candida) [8-9]. Due to the vital importance of these azole antifungals several methods have been reported for the determination of them either in pure forms, dosage forms, or biological fluids like chromatography [10-16], spectrophotometric [17-20], electrometric [21-22]. Structure investigation is an important part of drug development due to the need to identify the low level of impurities and degradation of drugs. The first step in drugs characterization is to establish the precise chemical identity. IR spectroscopy is an important and popular tool for structural elucidation and compound identification. To achieve an idea about the groups shared information of these solid ion-pairs, the IR spectra are compared with those of the drugs under study and the reagent [23-25]. Spectroscopic techniques, such as MS, in addition to thermal analyses (TG/DTG and DTA), are sensitive

*Corresponding author e-mail: mazayed429@yahoo.com

Received 13/4/2019; Accepted 14/5/2019

DOI: 10.21608/EJCHEM.2019.11907.1750

©2019 National Information and Documentation Center (NIDOC)

tools for such purposes. Therefore, the structures of the solid ion-pairs are investigated by these analytical techniques. MS and thermal analysis (TA) are two physical methods of analysis that are often used in parallel with each other [26-28]. The complementary nature of these techniques has been demonstrated for some species; where the fragmentation and/or subsequent degradation processes began at a similar location within the molecule i.e. the weakest bond. In MS, the species are ionized, where ions of increased stability are detected. In TA, the species are heated and decompose yielding mass losses until the sample is completely decomposed. The aim of the present work is focusing on further application of our previous work on various drugs [29]. In the present study, solid ion-pairs are under investigation by elemental, infrared spectra (FT-IR), mass spectrometry (MS) and thermal analysis (TA) measurements (TG/DTG and DTA). The biological activities of FLZ, VRZ, and BTZ drugs and their Rbeng solid ion pairs will be tested. The biological and medical activity of these drugs could be improved and changed by their reaction with Rbeng.

Experimental

Materials and reagents

Analytes

All chemicals used were of analytical reagent grade (AR), and of the highest purity available. They included FLZ (M.Wt. = 306.271 g mol⁻¹) provided by Amoun Pharmaceutical Co, (Egypt), VRZ (M.Wt. = 349.311 g mol⁻¹) provided by Mash Pharmaceutical Co, (Egypt), and BTZ (M.Wt. = 474.79 g mol⁻¹) provided by Sabaa Pharmaceutical Co, (Egypt) as working standards. Rbeng disodium salt reagent was supplied from BDH UK Chemicals Ltd, Poole, England. Absolute ethanol (99.8 %, Sigma Aldrich, Germany), methanol HPLC grad (□ 99.9 %, Sigma Aldrich, Germany), phosphoric acid (88 %, BDH, England), acetic acid (El Salam for chemical industries, Egypt), boric acid (ADWIC), annular sodium hydroxide (Merck, Germany) and distilled water, obtained from all glass equipment, were used.

Preparation of the solid drugs-reagent products (ion-pairs)

The solid ion-pairs of VRZ, FLZ, and BTZ nitrate drugs with Rbeng were prepared, by mixing of 50 mL solution of Rbeng solution (10⁻³ M) to 50 mL of (10⁻³ M) standard solutions

of VRZ, FLZ and BTZ. These mixtures were adjusted to pH = 2 by adding 5 mL of universal buffer for each solution. The resulted solid ion-pairs appeared as precipitates. The obtained solid ion-pairs were filtered, washed with the suitable solvent, dried and recrystallized from dimethylformamide (DMF). The melting points of the separated crystalline ion-pairs were measured.

Instruments

The elemental analyses (EA) of these compounds for C, H, and N were made at the Micro-Analytical Center of Cairo University using automatic CHN instrument (Elementar CHNS analyser, model Vario EL III).

The FT-IR spectra were recorded on Thermo Electron Corporation, Madison, WI 53711, USA in range of 4000-400 cm⁻¹. The spectral resolution is ± 2 cm⁻¹ and spectrometer using KBr disc technique.

EI mass spectrum (MS) was obtained using Thermo Finnegan TRACE DSQ quadruple mass spectrometer with electron multiplier detector equipped with GCMS data system. The direct probe (DP) for solid material was used in this study. The sample was put into a glass sample micro-vial, by a needle (□ 1 µg max), the vial installed on the tip of the DP containing heating cable and inserted into the evacuated ion source. The sample was ionized by an electron beam emitted from the filament, the generated ions being effectively introduced into the analyser by the focusing and extractor lenses system. The mass spectrum was continuously scanned, and the obtained spectra were stored. EI mass spectra were obtained at ionizing energy value of 70 and 15 eV, ionization current of 60 µA and vacuum is better than 10⁻⁶ torr. The mass fragmentation schemes of the drugs have been proposed according to EI mass spectra at 70 eV.

The thermal analyses (TG/DTG and DTA) were made using Shimadzu system of DTG-60H thermal analysers. These instruments were calibrated using indium metal as a thermally stable material. The mass losses of the samples from 5 to 10 mg and heat responses of the change of the samples were measured from room temperature up to 800 °C. The thermal analyses were carried out in a dynamic nitrogen atmosphere 20 mL min⁻¹ with a heating rate of 10 °C min⁻¹. The proposed thermal decomposition schemes of the tested compounds have been proposed according to the obtained thermograms.

Biological activity of the drugs and their ion-pairs

The antimicrobial activity of the drugs and their ion-pairs was determined using agar well diffusion method [30]. All the compounds were tested in vitro for their antibacterial activity against *staphylococcus aureus* and *Streptococcus mutans* (Gram positive bacteria), *Escherichia coli*, *Pseudomonas aeruginosa* and *klebsiella* (Gram negative bacteria) using nutrient agar medium. Ampicillin and Gentamicin were used as standard drugs for Gram positive and Gram negative respectively. DMSO was used as solvent control. The compounds were tested at a concentration of 15 mg/mL against both bacterial and fungal strains.

The sterilized media was poured onto the sterilized Petri dishes (20 - 25 mL, each petri dish) and allowed to solidify at room temperature. Microbial suspension was prepared in sterilized saline equivalent to McFarland 0.5 standard solution (1.5x 10⁵ CFU mL⁻¹) and its turbidity was adjusted to OD= 0.13 using spectrophotometer at 625 nm. Optimally, within 15 minutes after adjusting the turbidity of the inoculum suspension, a sterile cotton swab was dipped into the adjusted suspension and was flooded on the dried agar surface then allowed to dry for 15 minutes with lid in place. Wells of 6 mm diameter was made in the solidified media with the help of sterile borer. 100 µL of

the solution of the tested compound was added to each well with the help of micropipette. The plates were incubated at 37°C for 24 hrs in case of antibacterial activity. This experiment was carried out in triplicate and zones of inhibition were measured in mm. scale.

Results and Discussion

This study aims chiefly to confirm the proposed schemes and stoichiometry of the reaction between the drugs under study and Rbeng reagent by separation and identification of the formed ion-pairs.

During application of the proposed method using Rbeng reagent for spectrophotometric micro determination of the selected drugs, the formation of solid ion-pairs is detected, particularly in high concentrations of drug solutions. These solid ion-pairs are prepared, separated and their structures were elucidated by EA, FT-IR, MS and Thermal analysis.

Elemental analysis (EA) of the solid ion-pairs

EA of the prepared solid ion-pairs is performed. The elemental analyses results, analytical and physical data of Rbeng - drug ion-pairs are given in Table (1). From these data; the general formulae of the formed solid ion-pairs are determined, and their mole masses are calculated.

TABLE 1. Analytical and physical data of Rbeng-drug ion – pairs.

Ion-pair	R: D	m. p (°C)	Elemental analysis Calculated (Found %)		
			C	H	N
VRZ – Rbeng (C ₃₆ H ₁₈ Cl ₄ F ₃ I ₄ N ₅ O ₆) Mol. Mass = 1323	1:1	308.8	32.6 (31.6)	1.3 (2.2)	5.3 (5.1)
FLZ - Rbeng (C ₃₃ H ₁₆ Cl ₄ F ₂ I ₄ N ₆ O ₆) Mol. Mass=1277.9	1:1	307.9	30.9 (29.8)	1.25 (1.56)	6.6 (6.5)
BTZ – Rbeng (C ₃₉ H ₂₁ Cl ₇ I ₄ N ₂ O ₅ S) Mol. Mass = 1385.4	1:1	257.9	33.7 (32.5)	1.5 (2.08)	2.1 (2.5)

Rbeng (C₂₀H₂C₁₄O₅, mol mass = 971.66 g mol⁻¹), VRZ drug (C₁₆H₁₄F₃N₅O, mol mass = 349.311 g mol⁻¹), BTZ drug (C₁₉H₁₈C₁₃N₃O₃S, mol mass = 474.72 g mol⁻¹), FLZ drug (C₁₃H₁₂F₂N₆O, mol mass = 306.271 g mol⁻¹).

FT-IR analysis of the solid ion-pairs

Infrared spectrum of VRZ and its solid ion-pair

The IR spectra of VRZ drug, Rbeng reagent and their solid ion-pair are achieved in the wavenumber range 4000 – 400 cm^{-1} , as shown in Fig. 1 & 2(a, b). The FT-IR of Rbeng (Fig. 1) refers to the bands of $\text{C}=\text{O}$ stretching of the carboxylate at 1615.07 cm^{-1} and $\text{C}-\text{O}$ stretching of the carboxylate at 951.53 cm^{-1} . These bands are shifted to higher values of wavenumber in the corresponding VRZ–Rbeng

ion-pair (Fig. 2b), $\text{C}=\text{O}$ stretching of the carboxylate at 1770.79 cm^{-1} and $\text{C}-\text{O}$ stretching of the carboxylate at 958.54 cm^{-1} [23-25]. The FT-IR of VRZ (Fig. 2a) refers to the bands of $\text{C}=\text{C}$ stretching of the aromatic at 1590.57 cm^{-1} and $\text{C}-\text{N}$ stretching at 1280.8 cm^{-1} . These bands are shifted to higher value of wavenumber ($\text{C}=\text{C}$ stretching of the aromatic at 1595.47 cm^{-1} and lower wavenumber $\text{C}-\text{N}$ stretching at 1203.2 cm^{-1} in the corresponding VRZ–Rbeng ion-pair (Fig. 2b) [31].

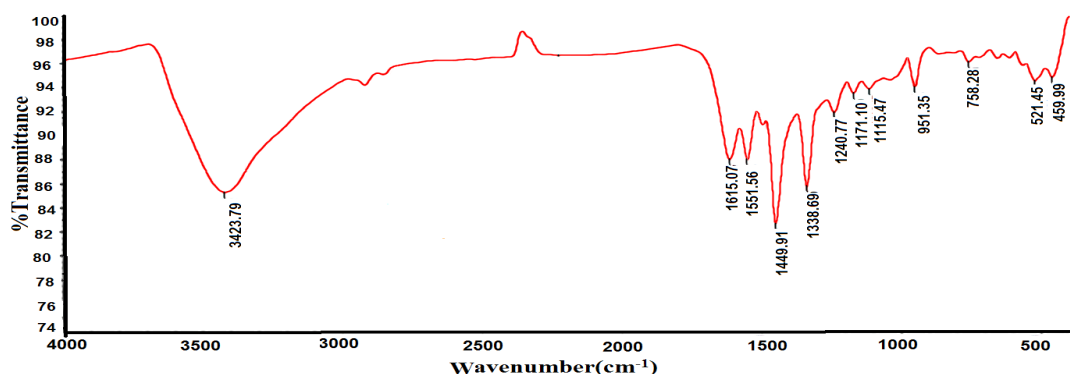


Fig. 1. FT-IR Spectrum of solid Rbeng reagent.

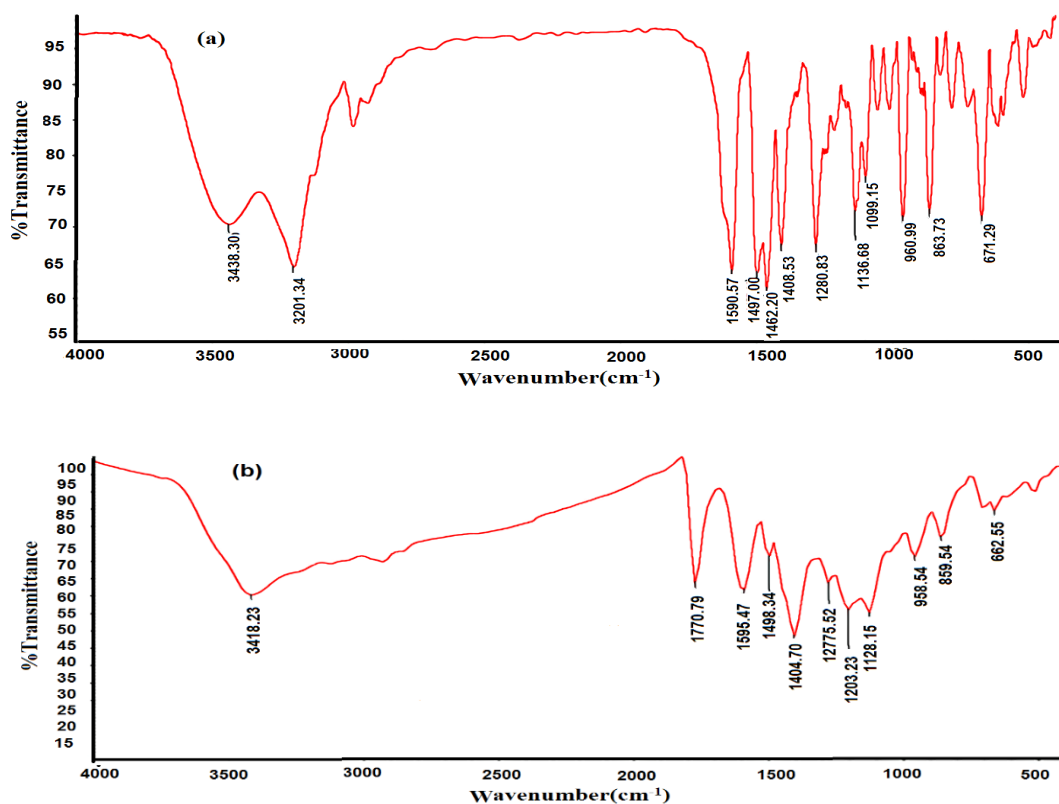


Fig. 2. FT-IR Spectrum of (a) Solid VRZ drug, (b) Solid VRZ – Rbeng ion – pair.

Infrared spectrum of FLZ and its solid ion-pair

The IR spectra of FLZ drug and their solid ion-pair with Rbeng were achieved in the wavenumber range 4000 – 400 cm^{-1} , as shown in Fig. 3(a, b). The FT-IR of Rbeng (Fig. 1) refers to the bands of $\square(\text{C}=\text{O})$ stretching of the carboxylate at 1615.07 cm^{-1} and $\square(\text{C}-\text{O})$ stretching of the carboxylate at 951.53 cm^{-1} . These bands are shifted to higher values of wavenumber in the corresponding FLZ – Rbeng ion-pair (Fig. 3b), $\square(\text{C}=\text{O})$ stretching of the carboxylate at 1766.7 cm^{-1} and $\square(\text{C}-\text{O})$ stretching of the carboxylate at 960.7 cm^{-1} [23-25]. The FT-IR of FLZ (Fig. 3a) refers to the bands of $\square(=\text{C}-\text{H})$ and $\square(\text{C}=\text{C})$ stretching of the aromatic ring at 3115.27 and 1621.29 cm^{-1} , $\square(\text{C}-\text{N})$ stretching of triazole ring at 1213.89 cm^{-1} [32]. These bands are shifted to lower values of wavenumber in the corresponding FLZ – Rbeng ion-pair (Fig. 3b), $\square(=\text{C}-\text{H})$ and $\square(\text{C}=\text{C})$ stretching of the aromatic ring at 2926.87 and 1616.17 cm^{-1} and $\square(\text{C}-\text{N})$ stretching of triazole ring at 1145.22 cm^{-1} .

Infrared spectrum of BTZ and its solid ion-pair

The IR spectra of BTZ drug and their solid ion-pair with Rbeng were achieved in the wavenumber range 4000 – 400 cm^{-1} , as shown in Fig. 4(a, b). The FT-IR of Rbeng (Fig. 1) refers to the bands of

$\square(\text{C}=\text{O})$ stretching of the carboxylate at 1615.07 cm^{-1} and $\square(\text{C}-\text{O})$ stretching of the carboxylate at 951.53 cm^{-1} . These bands are shifted to higher values of wavenumber in the corresponding BTZ – Rbeng ion-pair (Fig. 4b), $\square(\text{C}=\text{O})$ stretching of the carboxylate at 1768 cm^{-1} or to lower value of wavenumber for the $\square(\text{C}-\text{O})$ stretching of the carboxylate at 948.68 cm^{-1} [23-25]. The FT-IR of BTZ (Fig. 4a) $\square(=\text{C}-\text{H})$ and $\square(\text{C}=\text{C})$ stretching of the aromatic ring at 3130.61 and 1581.1 cm^{-1} and $\square(\text{C}-\text{N})$ stretching of Imidazole ring at 1318.07 cm^{-1} [33]. These bands are shifted to lower values of wavenumber in the corresponding BTZ–Rbeng ion-pair (Fig. 4b), $\square(\text{C}=\text{C})$ stretching of the aromatic ring and $\square(\text{C}-\text{N})$ stretching of imidazole ring of the aromatic ring at 1548.1 and 1188.22 cm^{-1} or to higher value of wavenumber $\square(=\text{C}-\text{H})$ of the aromatic ring at 3132.65 cm^{-1} .

Depending upon the FT-IR data previously discussed; the shift of the band's frequencies of some groups of the reagent and the drug into lower or higher wavenumbers may be attributed to the electrostatic attraction between the cationic drug and the anionic form of Rbeng reagent.

The proposed structures of the drugs – Rbeng solid ion pairs are given in Fig. 5.

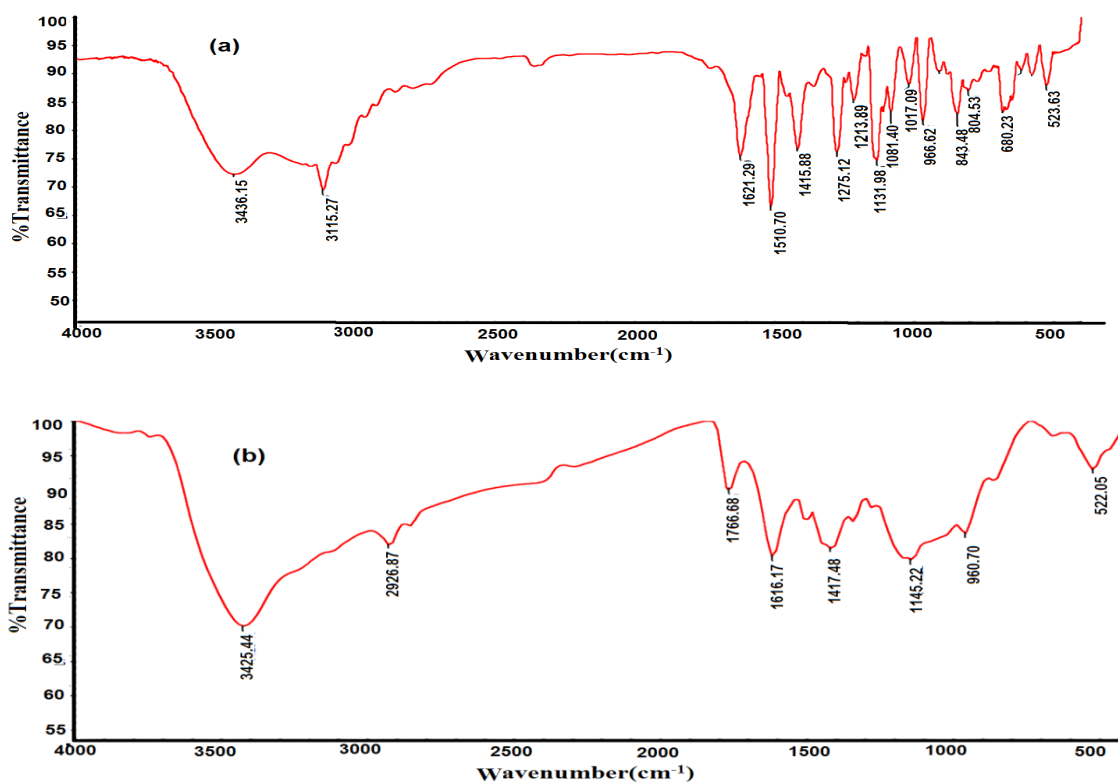


Fig. 3. FT-IR Spectrum of (a) Solid FLZ drug, (b) Solid FLZ – Rbeng ion – pair.

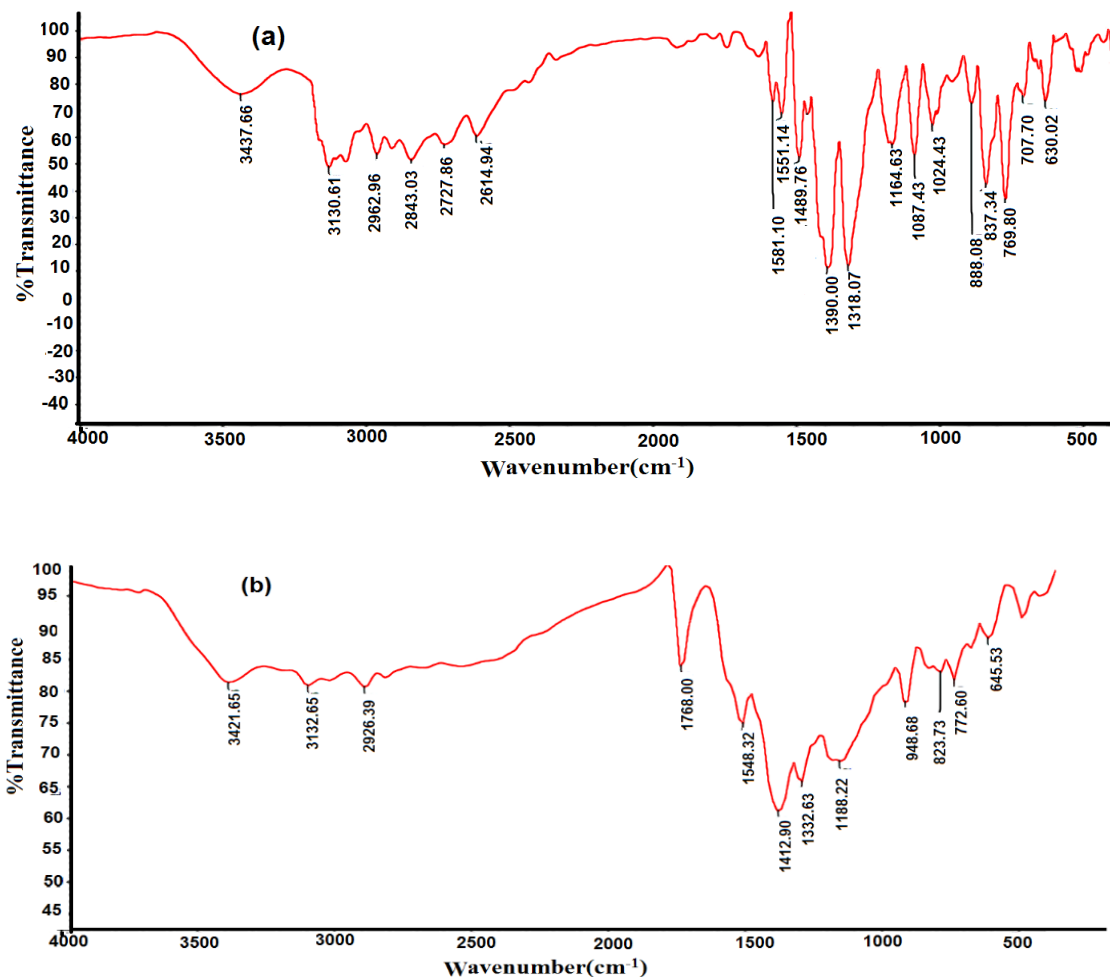


Fig. 4. FT-IR Spectrum of (a) Solid BTZ drug, (b) Solid BTZ – Rbeng ion – pair.

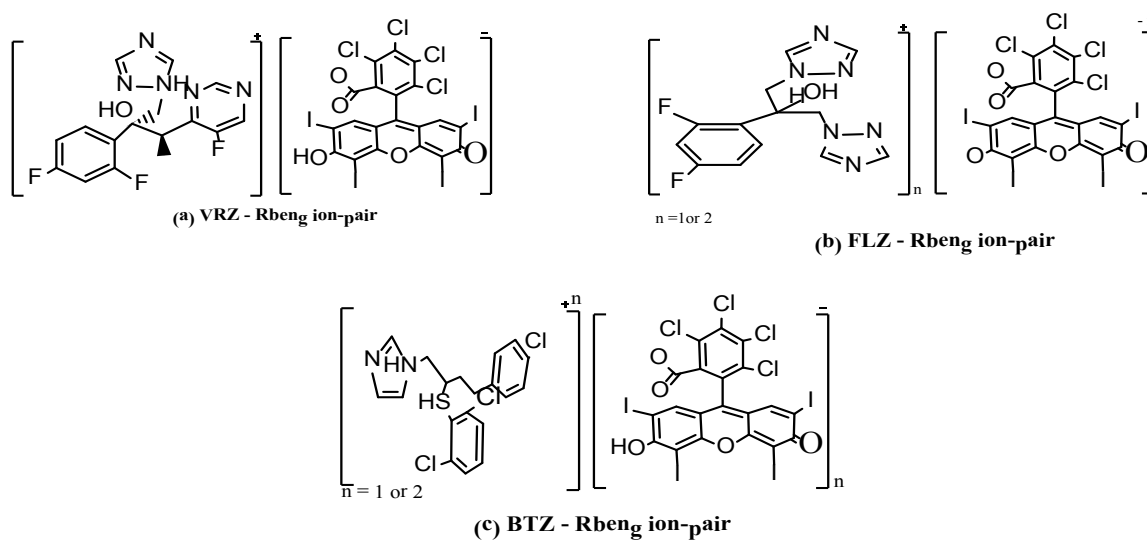


Fig. 5. The proposed structures of the drugs – Rbeng solid ion pairs.

Thermal and mass Structure characterization of drugs and their solid ion-pairs with Rbeng

Thermal analyses of VRZ drug

Thermogravimetric (TG/DTG) analysis of solid VRZ drug is employed to provide quantitative information on mass losses due to thermal decomposition as a function of time and temperature. The thermal analyses data of VRZ drug are shown in Fig. 6(a, b).

From TG/DTG thermograms (Fig. 6a) VRZ decomposed in one main step within temperature range 150 - 250 °C with practical total weight loss of 99.2 %. The main step at (150 – 250 oC) and exactly at 213.39 °C, may due to total decomposition of VRZ drug (Pract. % = 99.2 %, Calc. % = 100 %). This weight loss is confirmed

by the appearance of an endothermic peak in DTA (Fig. 6b) at temperature 232.76 °C. An endothermic peak appears in DTA at 129.99 °C, may be due to the melting of VRZ; which corresponds to the value of the reported melting point [34]. Exothermic peak in DTA appears at 521.66 °C; which may refer to chemical rearrangement and/or chemical recombination of the fragments to give the final products. The proposed thermal decomposition pathway of VRZ drug may be represented by Scheme 1.

Thermal analyses of VRZ – Rbeng ion-pair

The thermal analyses data of solid VRZ – Rbeng ion pair are shown in Fig. 7 (a,b).

From TG/DTG thermograms (Fig. 7a),

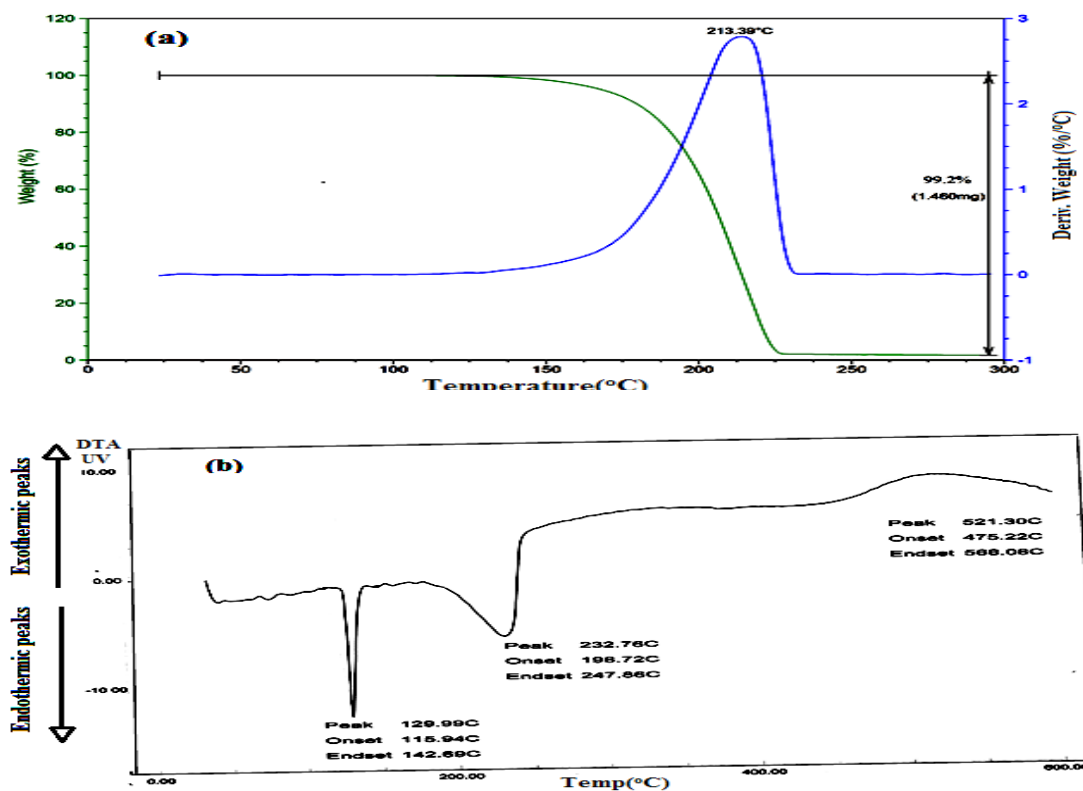
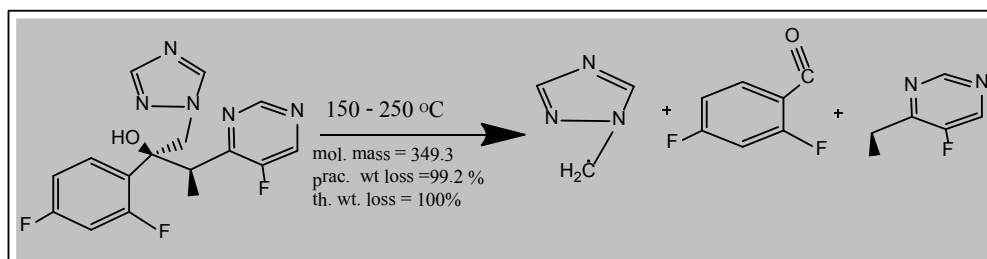


Fig. 6. Thermal analyses of VRZ drug (a) TGA/DTG, (b) DTA .



Scheme 1. Proposed thermal decomposition scheme of VRZ drug.

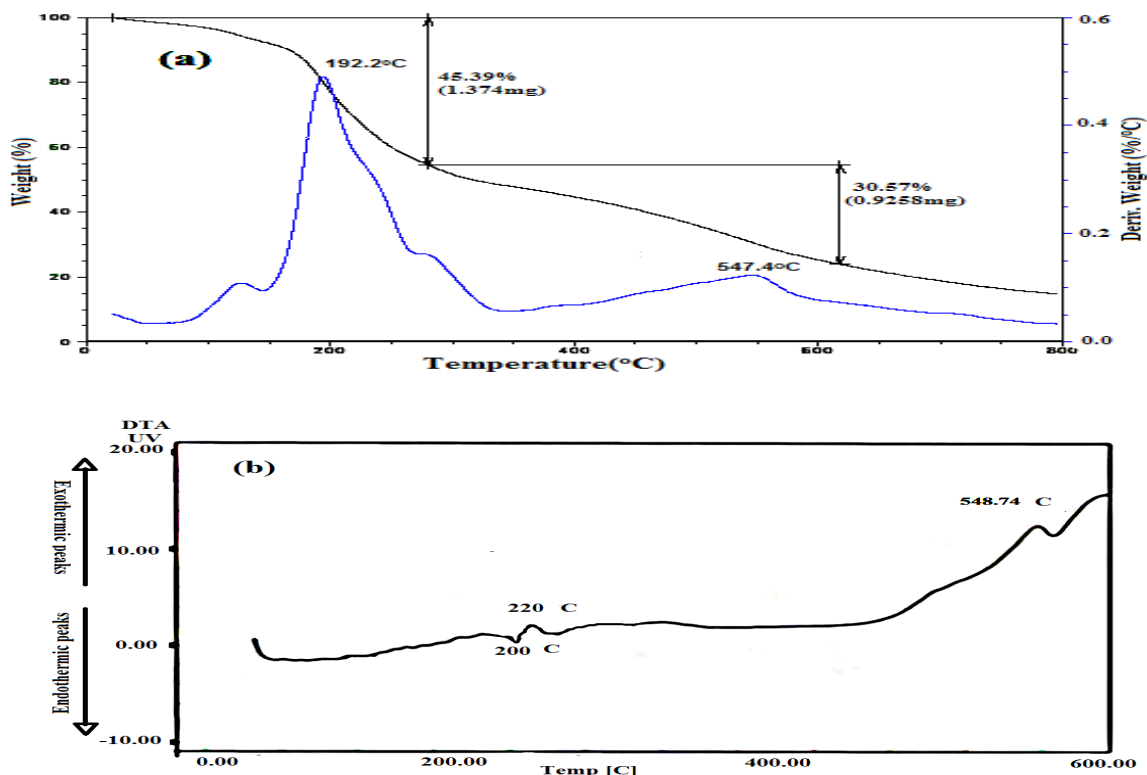
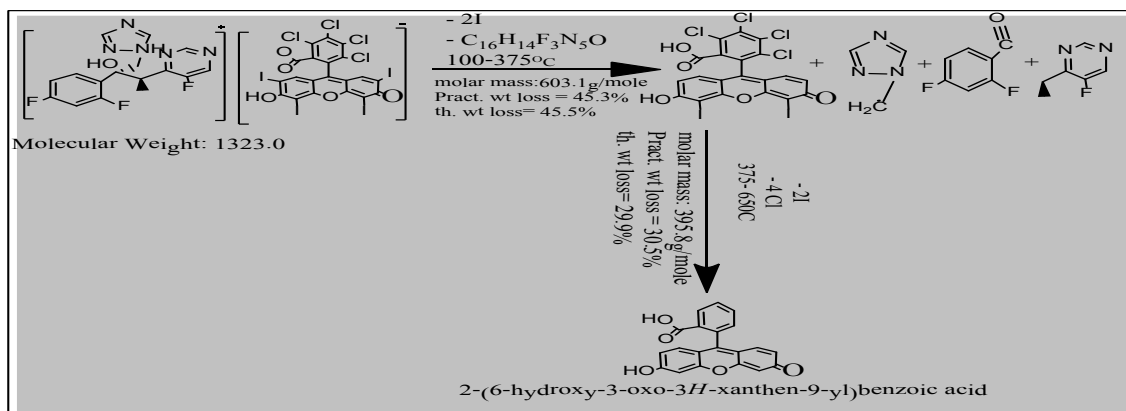


Fig. 7. Thermal analyses of VRZ – Rbeng ion-pair: (a) TGA/DTG, (b) DTA.

VRZ - Rbeng ion-pair decomposed into two main steps within temperature range 100 - 650 °C with a practical total weight loss of 75.96 %. The first step at 100 - 375 °C and exactly at 192.2 °C, may be related to decomposition of ion pair into two components, VRZ drug; which may be decomposed as a proposed (Scheme 1) and Rbeng reagent which loss 2I (Pract. % = 45.3 %, Calc. % = 45.5 %). These weight losses are confirmed by the appearance of an endothermic peak in DTA (Fig. 7b) at 200 °C and an exothermic in DTA at 220° C may be referred to chemical rearrangement

and/or chemical recombination of the fragments (2I to give I₂ molecule). The second step at 375 – 650 °C and exactly at 547.4 may be due to loss of 2I and 4Cl (Pract. % = 30.05 %, Calc. % = 29.9 %). This loss appears as an exothermic peak in DTA at 548.74°C; may refer to chemical rearrangement and/or chemical recombination of the fragments to give the final products (2I to give I₂ and 4Cl to give 2Cl₂ molecules). The proposed thermal decomposition pathway of VRZ – Rbeng ion-pair may be represented by Scheme 2.

Thermal analyses of FLZ drug



Scheme 2. Proposed thermal decomposition scheme of VRZ - Rbeng ion pair.

The thermal analyses data of FLZ drug are shown in Fig. 8(a, b).

From TGA and DTG thermograms (Fig. 8a), FLZ decomposed in one main step within temperature range 100 - 275 °C with a practical total weight loss of 99.03 %. The main step at (100 – 275 oC) and exactly at 246.9 °C, may due to total decomposition of FLZ drug (Pract. % = 99.03 %, Calc. % = 100%). This weight loss is confirmed by the appearance of an endothermic peak in DTA (Fig. 8b) at temperature 298.21 °C. An endothermic peak appears in DTA at 69.43 °C, may be due to

dehydration of water. Another endothermic peak appears in DTA at 139.80 °C, may be due to the melting of FLZ; which corresponds to the value of the reported melting point [35]. Exothermic peak in DTA at 369.39°C, may refer to chemical rearrangement and/or chemical recombination of the fragments to give the final products. The proposed thermal decomposition pathway of FLZ drug may be represented by Scheme 3.

Thermal analyses of FLZ – Rbeng ion-pair

The thermal analyses data of FLZ - Rbeng

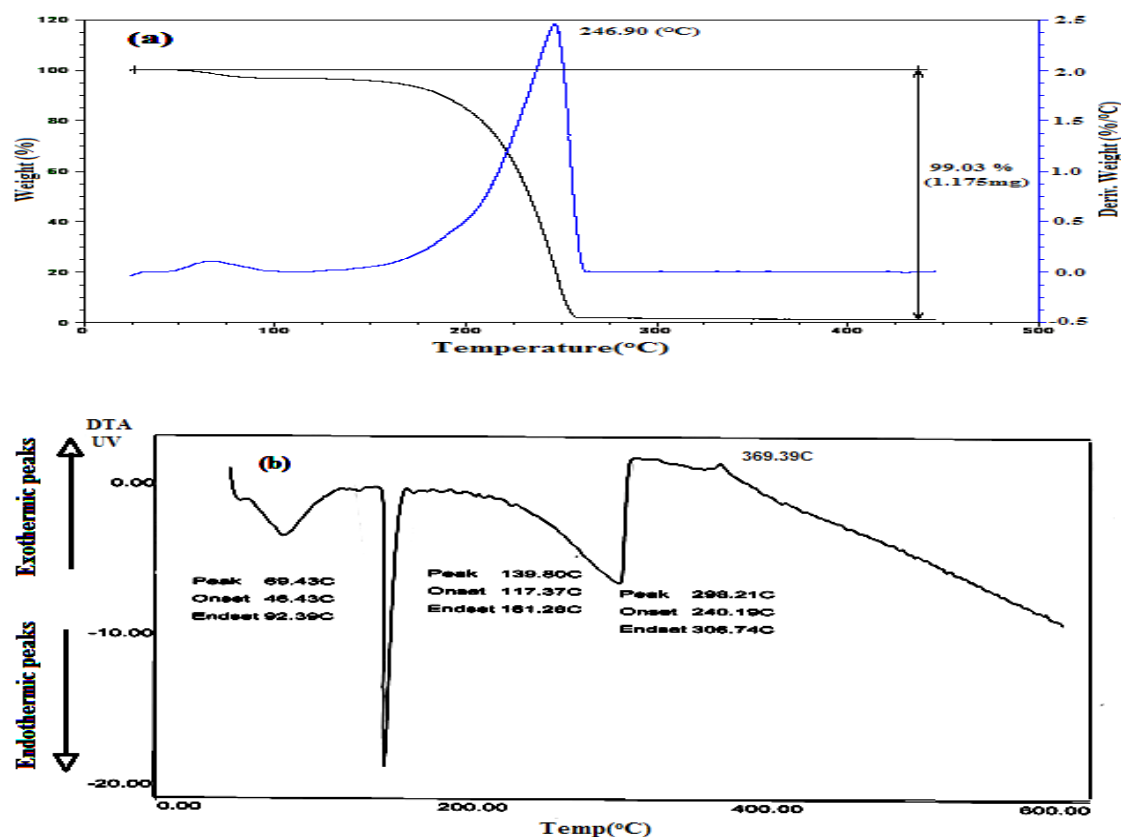
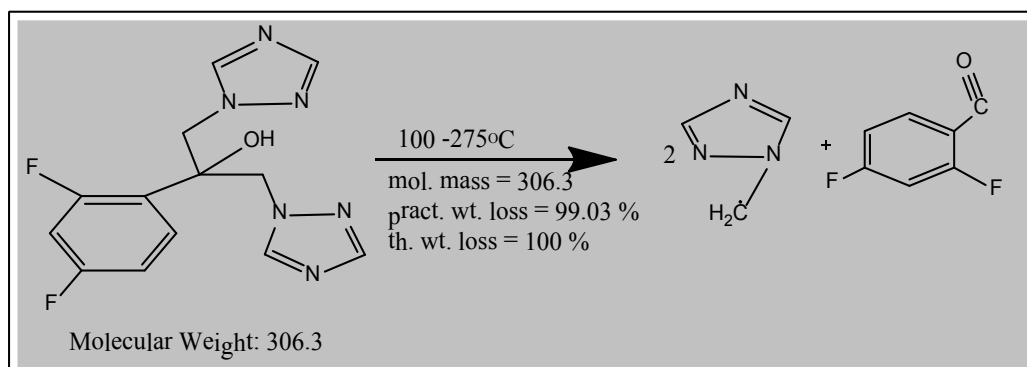


Fig. 8. Thermal analyses of FLZ drug (a) TGA/DTG, (b) DTA .



Scheme 3. Proposed thermal decomposition scheme of FLZ drug.

ion-pair are shown in Fig. 9(a, b).

From TGA and DTG thermograms (Fig. 9a), FLZ - Rbeng ion-pair decomposed into two main steps within temperature range 100 - 650 °C with a practical total weight loss of 73.44 %. The first step at (100 - 350 °C) and exactly at 243.58 °C, may be related to decomposition of ion pair into two components, FLZ drug; which may be decomposed as a proposed (Scheme 3) and Rbeng reagent which loss 2I (Pract. % = 43.4 %, Calc. % = 43.7 %). These weight losses are confirmed by the appearance of two exothermic peaks in DTA (Fig. 9b) at temperatures 198.39 °C and 302.34 °C,

may be referred to chemical rearrangement and/or chemical recombination of the fragments (2I to give I₂ molecule). The second step at (350 – 650 °C) and exactly at 516.75 °C, may be due to loss of 2I and 4Cl (Pract. % = 30.03 %, Calc. % = 30.9 %). This loss appears as an exothermic peak in DTA at 583.76 °C; which may refer to chemical rearrangement and/or chemical recombination of the fragments to give the final products (2I to give I₂ and 4Cl to give 2Cl₂ molecules). The proposed thermal decomposition pathway of FLZ – Rbeng ion-pair may be represented by Scheme 4.

Thermal analyses of BTZ drug

The thermal analyses data of BTZ drug are

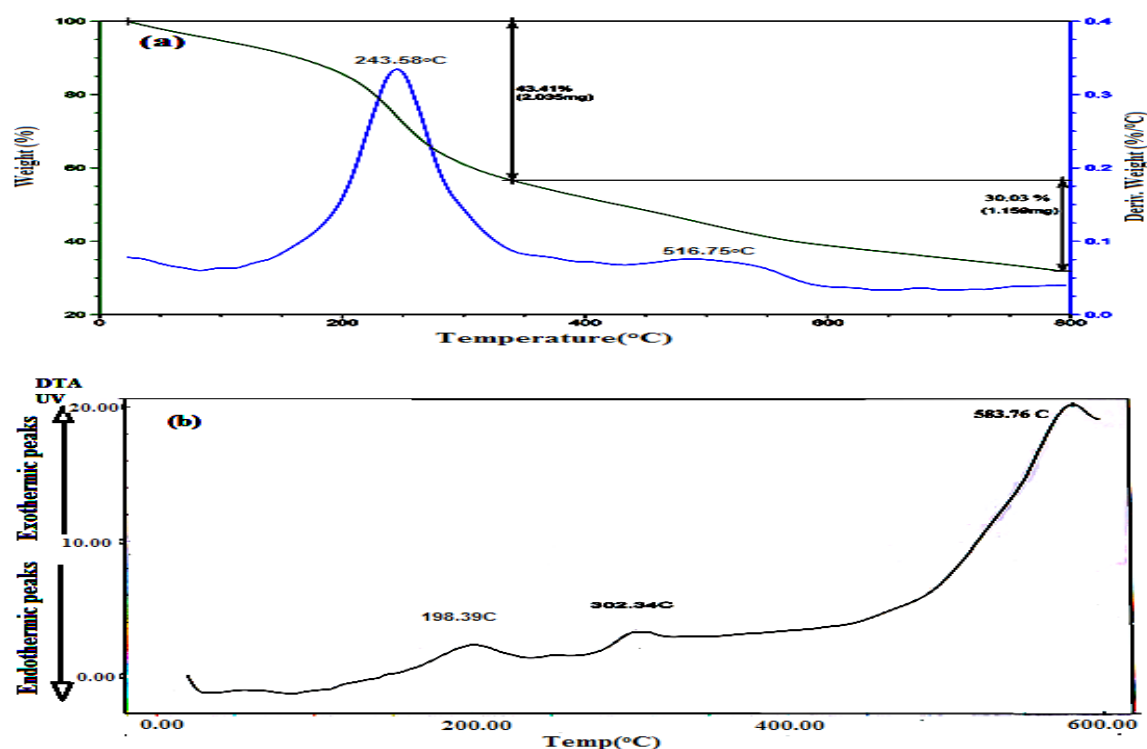
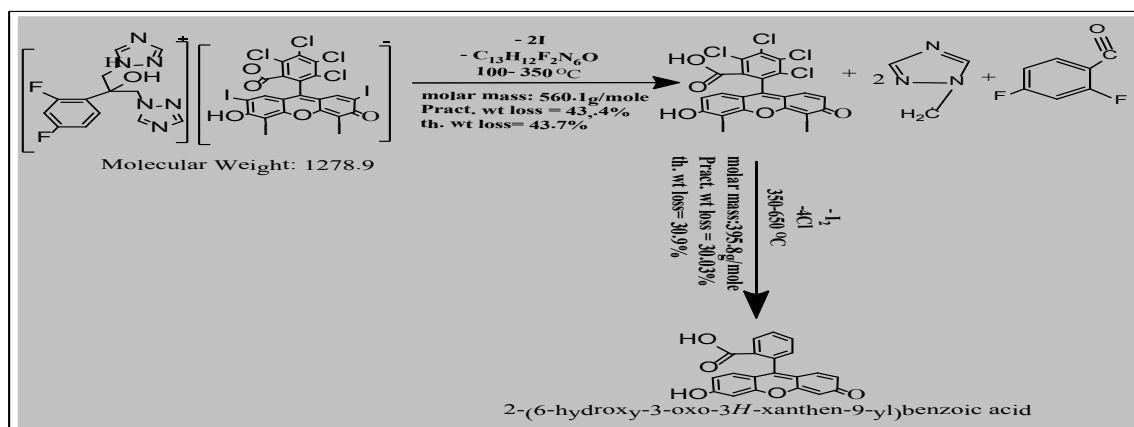


Fig. 9. Thermal analyses of FLZ – Rbeng ion-pair: (a)TGA/DTG, (b) DTA.



Scheme 4. Proposed thermal decomposition scheme of FLZ - Rbeng ion-pair.

shown in Fig. 10(a, b).

From TGA and DTG thermograms (Fig. 10a), BTZ decomposed in two main steps within temperature range 50 - 400 °C with a practical total weight loss of 86.5 %. The first step occurs at (50 – 250 °C) and exactly at 179.49 °C, this may be related to loss of HNO_3 (Pract. % = 13.24 %, Calc. % = 13.2%). This weight loss is confirmed by the appearance of an exothermic peak in DTA (Fig. 3.46b) at temperature 187.50 °C. The second step at (250 - 400 °C) and exactly at 300.75°C, this may be related to loss of $\text{C}_{16}\text{H}_{14}\text{Cl}_3\text{S}$ radical (Pract. % = 75.81 %, Calc. % = 75.4 %) and formation of 1H-imidazole. This weight loss is

confirmed by the appearance of an exothermic peak in DTA (Fig. 10b) at temperature 351.96 °C. An endothermic peak appears in DTA at 159.4 °C, may be due to the melting of BTZ; which corresponds to the value of the reported melting point [8]. The two exothermic peaks in DTA at 525.95 and 564.79 °C, may refer to chemical rearrangement and/or chemical recombination of the fragments to give the final products. The proposed thermal decomposition pathway of BTZ drug may be represented by Scheme 5.

Thermal analyses of BTZ – Rbeng ion-pair

The thermal analyses data of BTZ – Rbeng ion-pair are shown in Fig. 11(a, b).

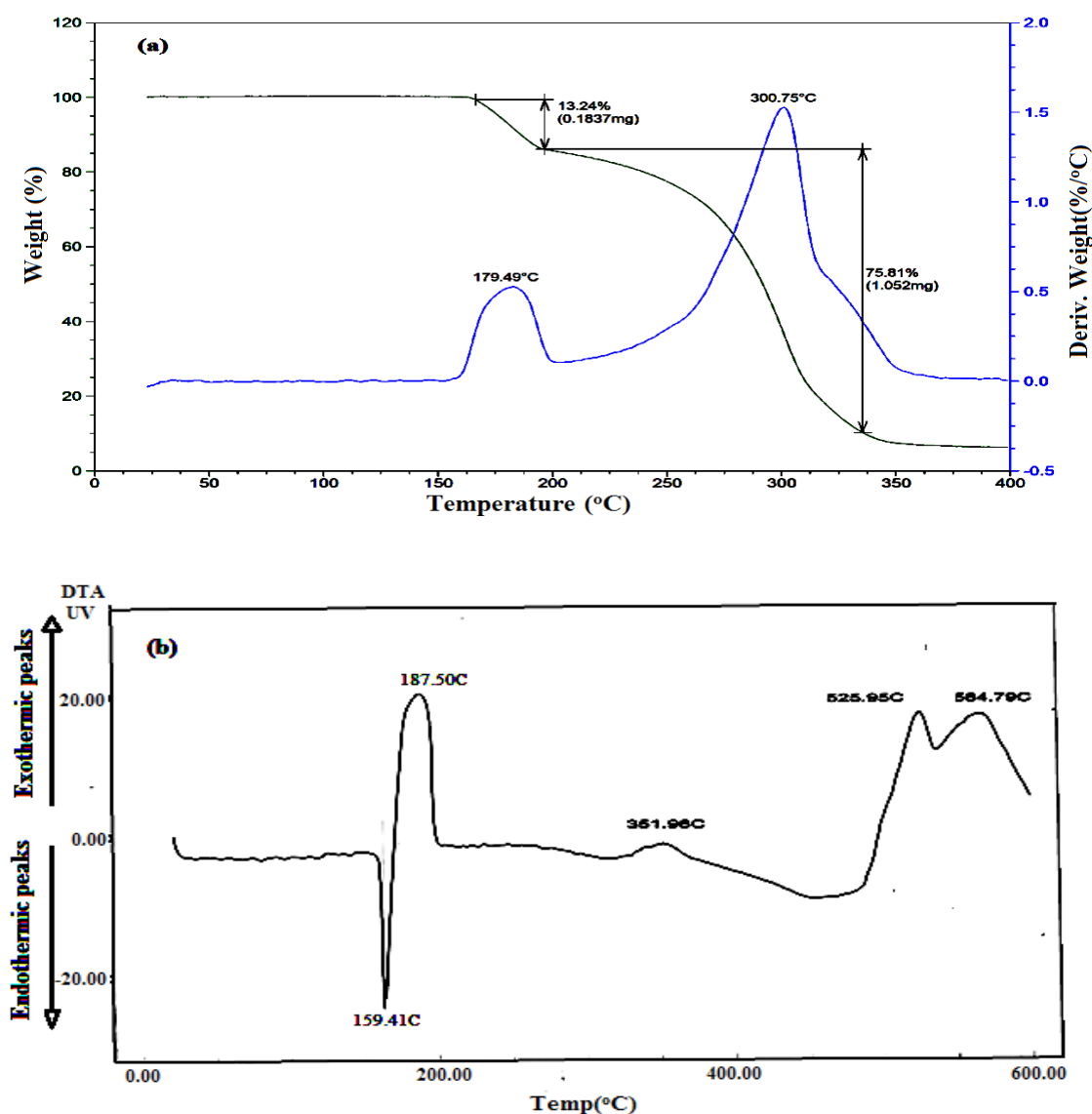
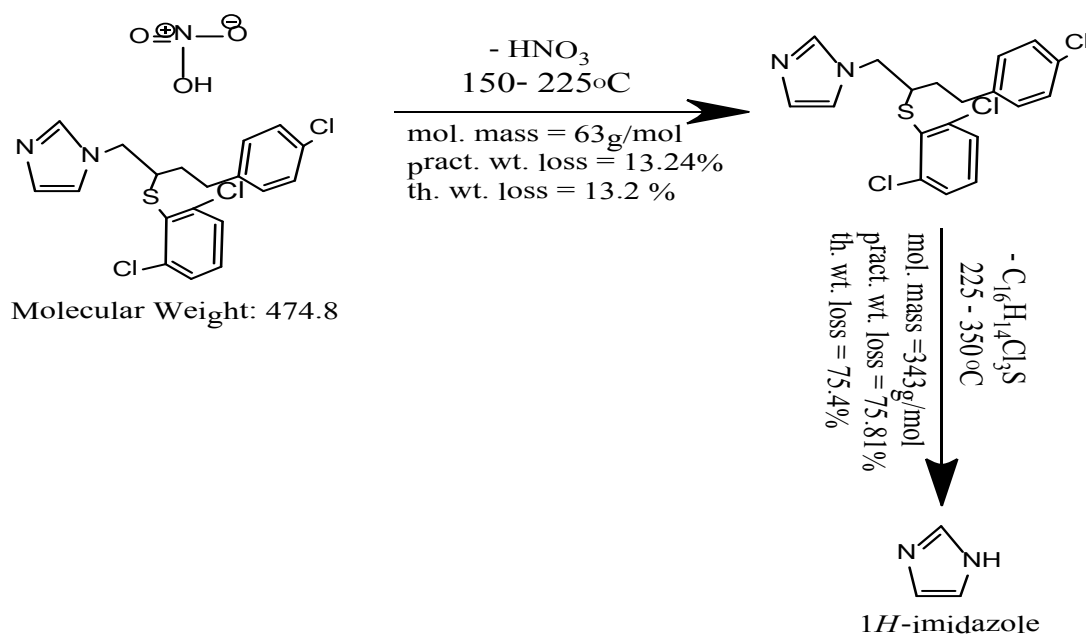


Fig. 10. Thermal analyses of BTZ drug: (a) TGA/DTG, (b) DTA.



Scheme 5. Proposed thermal decomposition scheme of BTZ drug.

From TGA and DTG thermograms (Fig. 11a), BTZ - Rbeng ion-pair decomposed into three main steps within temperature range 100 - 600 °C with a practical total weight loss of 75.00%. The first step at (100 - 250 °C) and exactly at 224.61°C, this may be related to loss of $\text{C}_{15}\text{H}_{13}\text{Cl}_3\text{S}$ radical (Pract. % = 23.41 %, Calc. % = 23.8 %). The second step at (250 - 400 °C) and exactly at 278.7 °C, this may be due to loss of $\text{C}_4\text{H}_6\text{N}_2$ and 2I (Pract. % = 23.59 %, Calc. % = 24.4 %). These two weight losses are confirmed by the appearance of a broad exothermic peak in the temperature range 50 - 400 °C in DTA (Fig. 11b), may refer to chemical rearrangement and/or chemical recombination of the fragments to give the final products (2I to give I_2 molecule). The third step at (400 - 600) and exactly at 559.3 °C, this may be due to loss of 2I and 4Cl (Pract. % = 28 %, Calc. % = 28.5 %). This appears as two exothermic peaks in DTA at 526.28 and 573.75 °C, may refer to chemical rearrangement and/or chemical recombination of the fragments to give the final products 2I to give I_2 and 4Cl to give 2Cl_2 molecules). The proposed thermal decomposition pathway of BTZ-Rbeng ion pair may be represented by Scheme 6.

Mass spectra of solid drugs and their ion-pairs with Rbeng

EI mass spectra results of VRZ at 70

eV are illustrated in Fig. 12(a). The signal appeared at $m/z = 350$, mol. Mass = 349.3 of relative intensity (RI) = 49.5 % is related to the molecular ion $[\text{M}]^+$ of general formula $[\text{C}_{16}\text{H}_{14}\text{F}_3\text{N}_3\text{O}]^+$. The high intensity reflects the stability of the molecular ion of VRZ. The base peak in the spectrum that appears at $m/z = 267.1$ (RI = 100 %) is mainly due to the formation of fragment ions $[\text{C}_{13}\text{H}_{10}\text{F}_3\text{N}_2\text{O}]^+$. Other important ion observed in the mass spectra at $m/z = 141$ (RI = 92.46 %), at $m/z = 125.1$ (RI = 19.52 %) and at $m/z = 82.1$ (RI = 16.2 %), respectively. These fragment ions may be due to the formation of $[\text{C}_7\text{H}_7\text{F}_2\text{O}]^+$, $[\text{C}_6\text{H}_6\text{FN}_2]^+$ and $[\text{C}_3\text{H}_4\text{N}_3]^+$, respectively. Comparison of MS and TA (Scheme 1) refers to the good agreement between MS and TA techniques.

EI mass spectra results of VRZ - Rbeng ion-pair at 70 eV are illustrated in Fig 12(b). The base peak in the spectrum that appears at $m/z = 57$, mol. mass = 56.1 (RI = 100 %) is mainly due to the formation of fragment ions of the formula $[\text{C}_2\text{H}_4\text{N}_2]^+$. Other important ion observed in the mass spectra at $m/z = 678$ (RI) = 37.7 %, at $m/z = 643.4$ (RI = 16.28 %), at $m/z = 627.4$ (RI = 24.01 %), at $m/z = 515$, mol. mass = 514.5 (RI = 40.69 %), at $m/z = 596$ (RI = 24.17%), at $m/z = 551$, mol. mass = 552 (RI = 42.3 %), at $m/z = 469$, mol. mass = 470.1 (RI = 14.75 %),

at $m/z = 332$ (RI = 11.68 %), at $m/z = 126.9$ (RI = 9.75 %), at $m/z = 140$, mol. mass = 141 (RI = 10.8%), at $m/z = 82$, mol. mass = 83.1 (RI = 11.76%) and $m/z = 70$, mol. mass = 69.1 (RI = 57.01 %), respectively. These fragment ions may be due to the formation of $[C_{19}H_6C_{14}I_2O_3]^+$, $[C_{19}H_7C_{13}I_2O_3]^+$, $[C_{19}H_7C_{13}I_2O_2]^+$, $[C_{14}H_9ClI_2O_3]^+$, $[C_{20}H_7C_{14}IO_3]^+$, $[C_{19}H_7C_{14}IO_3]^+$, $[C_{20}H_8C_{14}O_5]^+$, $[C_{20}H_{12}O_5]^+$, $[I]^+$, $[C_7H_3F_2O]^+$, $[C_3H_4N_3]^+$ and $[C_2H_3N_3]^+$, respectively. Comparison of MS and TA (Scheme 2) refers to the good agreement between MS and TA techniques.

EI mass spectra results of FLZ at 70 eV are illustrated in Fig. 12(c). The signal appeared at $m/z = 307$, mol. mass = 306.1 of relative intensity (RI) = 54.2 % is related to the molecular ion $[M]^+$ of general formula $[C_{13}H_{12}F_2N_6O]^+$. The high intensity reflects the stability of the molecular ion of FLZ. The base peak in the spectrum that appears at $m/z = 224.1$ (RI = 100 %) is mainly due to the formation of fragment ions of the formula $[C_{10}H_8F_2N_3O]^+$. Other important ion observed in the mass spectra at $m/z = 141$ (RI = 11.84 %), at $m/z = 127$ (RI = 38.3 %), at $m/z = 82$, mol. mass = 83.1 (RI = 52.98 %), respectively. These fragment ions may be due to the formation of $[C_7H_3F_2O]^+$, $[C_5H_9N_3O]^+$ and $[C_3H_5N_3]^+$, respectively. Comparison of MS and TA (Scheme 3) refers to the good agreement between MS and TA techniques.

EI mass spectra results of FLZ - Rbeng ion-pair at 70 eV are illustrated in Fig. 12(d). The base peak in the spectrum that appears at $m/z = 678$ (RI = 100 %) is mainly due to the formation of fragment ions of the formula $[C_{19}H_6C_{14}I_2O_3]^+$. Other important ion observed in the mass spectra at $m/z = 723$, mol. mass = 721.9 (RI = 11.77 %), at $m/z = 642$, mol. mass = 643.4 (RI = 75.3 %), at $m/z = 515$, mol. mass = 514.5 (RI = 25.61 %), at $m/z = 551$, mol. mass = 552 (RI = 94.9 %), at $m/z = 425$, mol. mass = 425.5 (RI = 15.87 %), at $m/z = 332$ (RI = 8.19 %), at $m/z = 141$ (RI = 7.83%), at $m/z = 82$, mol. mass = 83.1 (RI = 44.28 %), at $m/z = 70$, mol. mass = 69.1 (RI = 15.11 %) and at $m/z = 55$, mol. mass = 56.1 (RI = 49.09 %), respectively. These fragment ions may be due to the formation of $[C_{20}H_6C_{14}I_2O_5]^+$, $[C_{19}H_7C_{13}I_2O_3]^+$, $[C_{14}H_9ClI_2O_3]^+$, $[C_{19}H_7C_{14}IO_3]^+$, $[C_{14}H_8C_{13}IO]^+$, $[C_{20}H_{12}O_5]^+$, $[C_7H_3F_2O]^+$, $[C_3H_4N_3]^+$, $[C_2H_3N_3]^+$

and $[C_2H_4N_2]^+$, respectively. Comparison of MS and TA (Scheme 4) refers to the good agreement between MS and TA techniques.

EI mass spectra results of BTZ at 70 eV are illustrated in Fig. 12(e). The signal appeared at $m/z = 474.8$ of relative intensity (RI) = 54.4 % is related to the molecular ion $[M]^+$ of general formula $[C_{19}H_{18}C_{13}N_3O_3S]^+$. The high intensity reflects the stability of the molecular ion of BTZ. The base peak in the spectrum that appears at $m/z = 125$, mol. mass = 126.6 (RI = 100 %) is mainly due to the formation of fragment ions of the formula $[C_7H_6Cl]^+$. Other important ion observed in the mass spectra at $m/z = 412$ (RI = 26.88%), at $m/z = 377.3$ (RI = 64.91 %), at $m/z = 151$, mol. mass = 152.3 (RI = 21.08 %), at $m/z = 89$, mol. mass = 90.2 (RI = 46.33%), at $m/z = 81$, mol. mass = 82.1 (RI = 59.91%), at $m/z = 69$, mol. mass = 68.1 (RI = 66.24%) and $m/z = 55$, mol. mass = 56.1 (RI = 52.09 %), respectively. These fragment ions may be due to the formation of $[C_{19}H_{17}C_{13}N_2S]^+$, $[C_{19}H_{18}C_{12}N_2S]^+$, $[C_7H_6Cl]^+$, $[C_4H_9S]^+$, $[C_4H_5N_2]^+$, $[C_3H_5N_2]^+$ and $[C_2H_4N_2]^+$, respectively. Comparison of MS and TA (Scheme 5) refers to the good agreement between MS and TA techniques.

EI mass spectra results of BTZ - Rbeng ion-pair at 70 eV are illustrated in Fig. 12(f). The base peak in the spectrum that appears at $m/z = 377.3$ (RI = 100 %) is mainly due to the formation of fragment ions of the formula $[C_{19}H_{18}C_{12}N_2S]^+$. Other important ion observed in the mass spectra at $m/z = 642$, mol. mass = 643.4 (RI = 12.07 %), at $m/z = 551$, mol. mass = 552 (RI = 17.29 %), at $m/z = 411.8$ (RI = 58.15 %), at $m/z = 254$, mol. mass = 253 (RI = 80.87 %), at $m/z = 89$, mol. mass = 90.2 (RI = 9.44 %), at $m/z = 82.1$ (RI = 18.83 %) and $m/z = 69$, mol. mass = 68.1 (RI = 20.34 %), respectively. These fragment ions may be due to the formation of $[C_{19}H_7C_{13}I_2O_3]^+$, $[C_{19}H_7C_{14}IO_3]^+$, $[C_{19}H_{17}C_{13}N_2S]^+$, $[C_{13}H_{10}C_{12}O]^+$, $[C_4H_{10}S]^+$, $[C_4H_6N_2]^+$ and $[C_3H_4N_2]^+$, respectively. Comparison of MS and TA (Scheme 6) refers to the good agreement between MS and TA techniques.

Biological activity of the drugs and their ion pairs

The antimicrobial activity of synthesized VRZ, FLZ, BTZ and their ion pairs was determined using agar well diffusion method

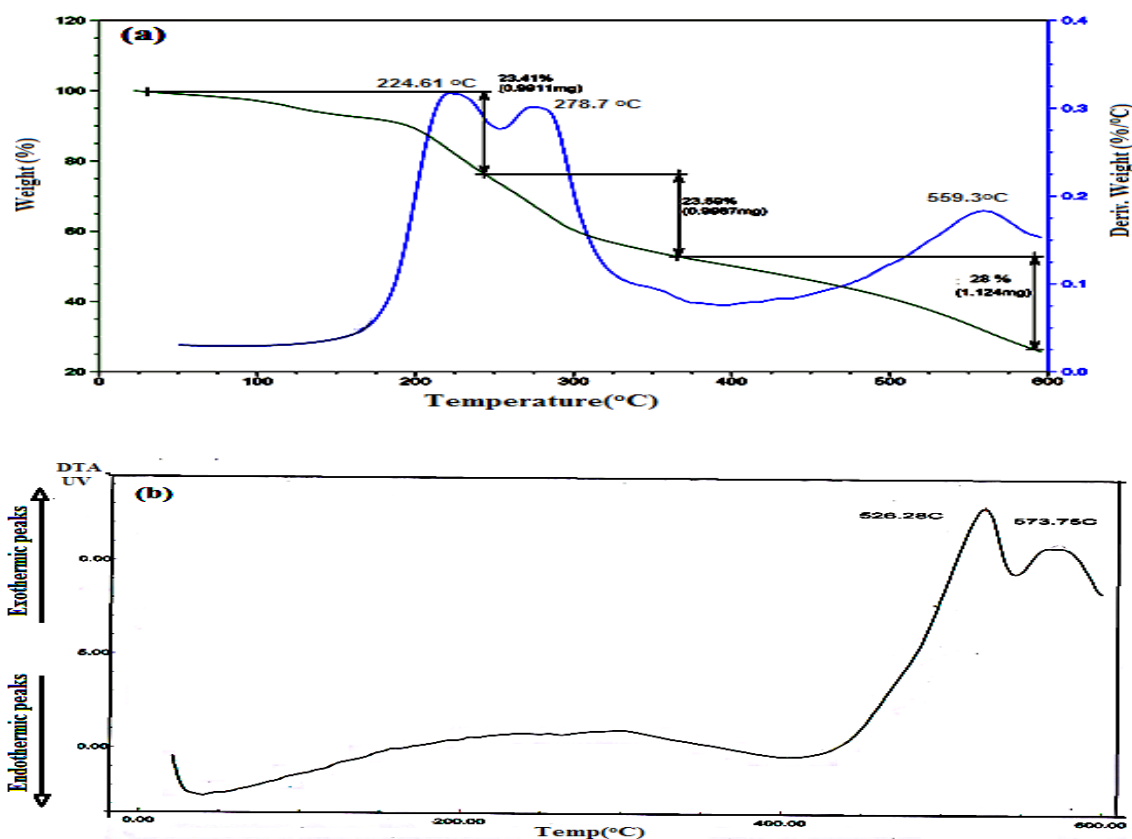
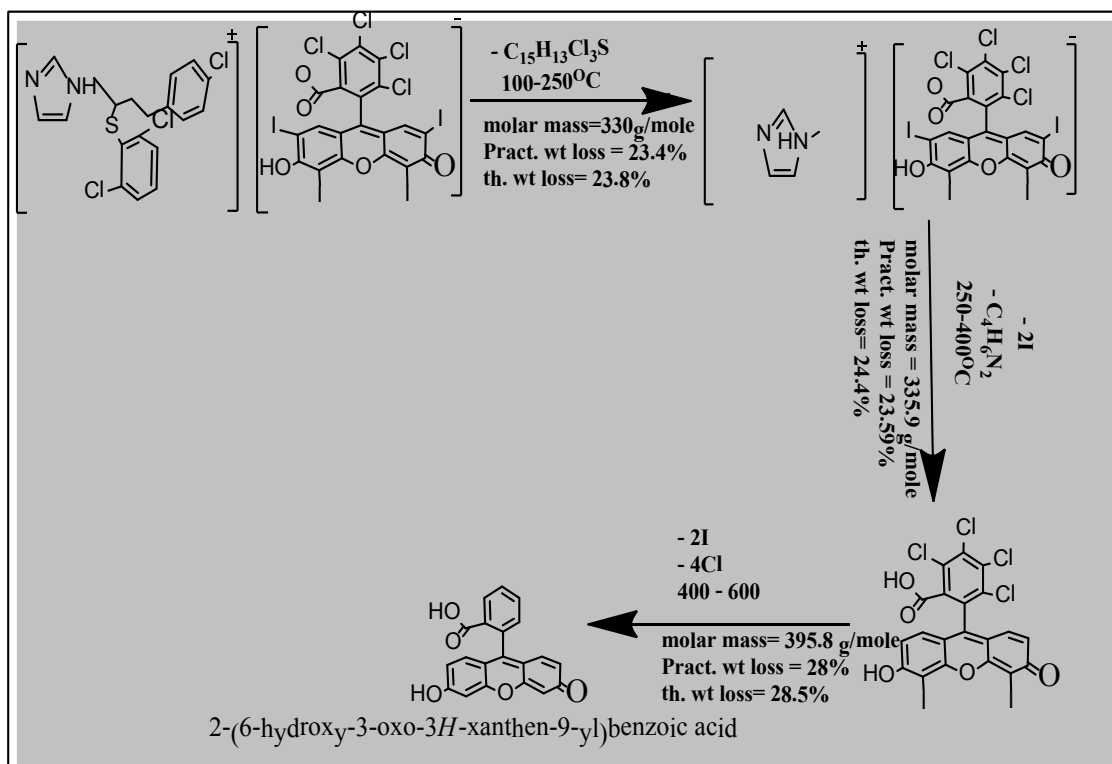
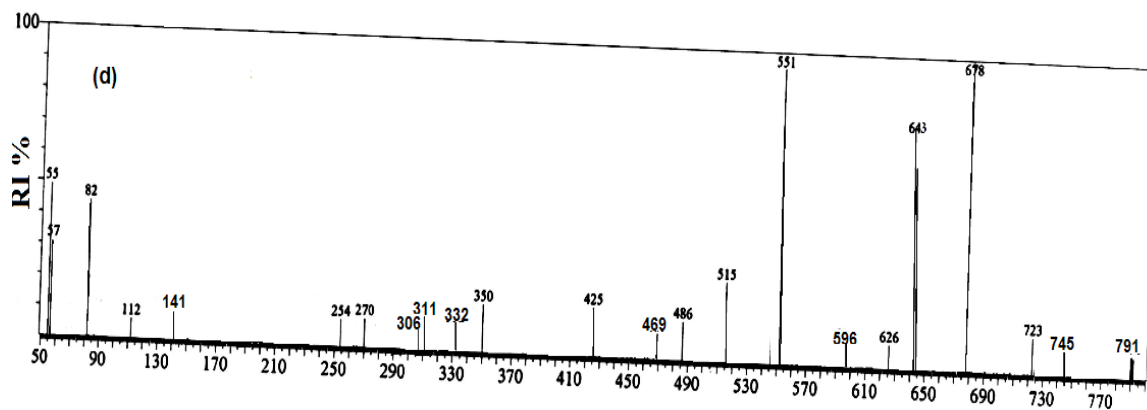
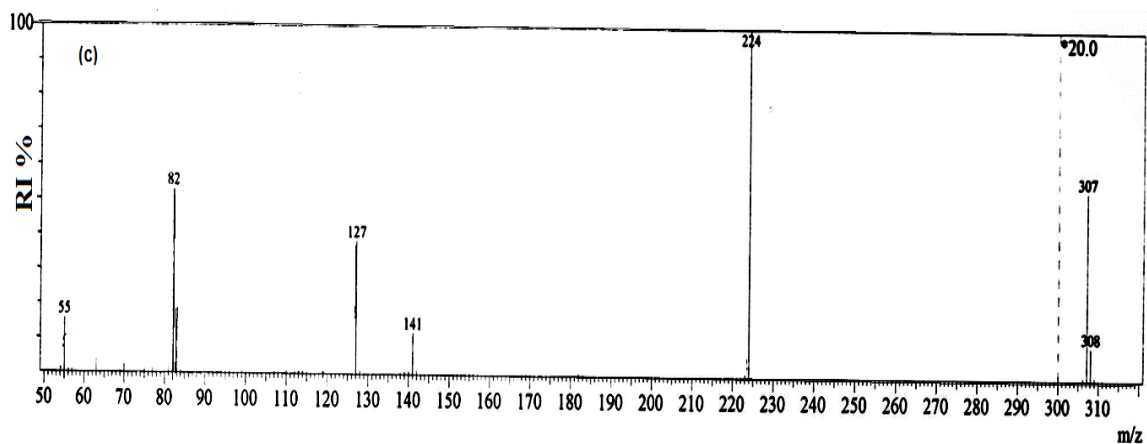
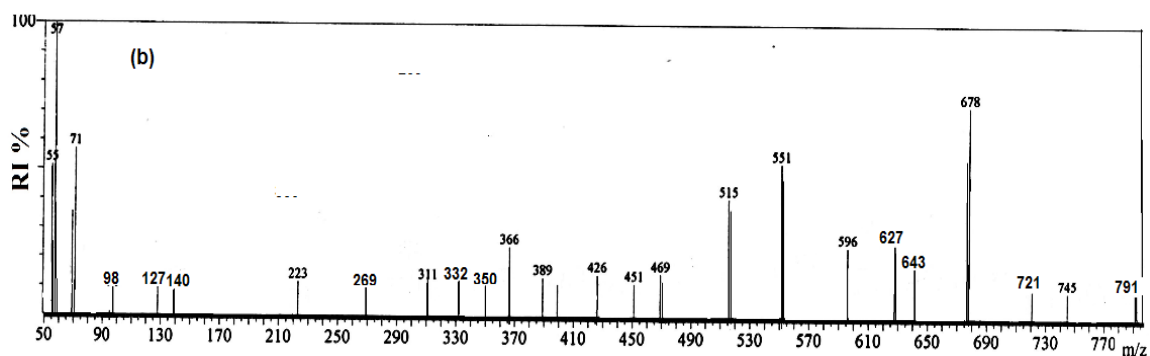
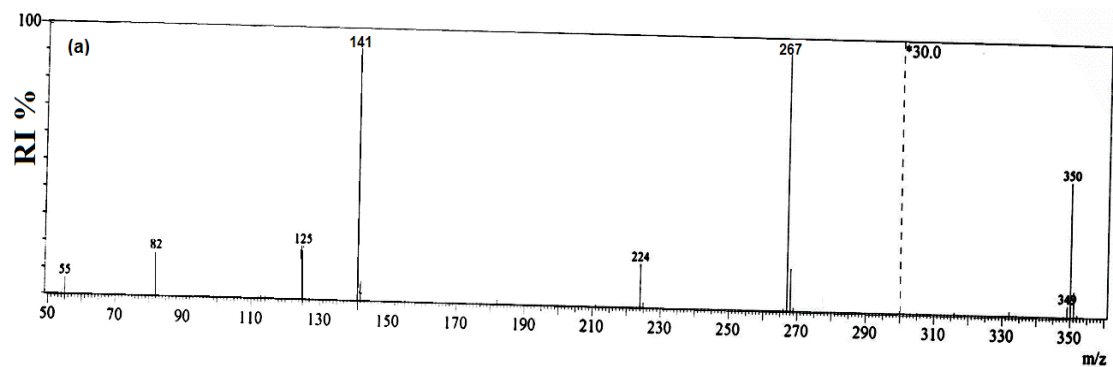


Fig. 11. Thermal analyses of BTZ -Rbeng ion-pair (a)TGA/DTG, (b) DTA .



Scheme 6. Proposed thermal decomposition scheme of BTZ – Rbeng ion-pair.



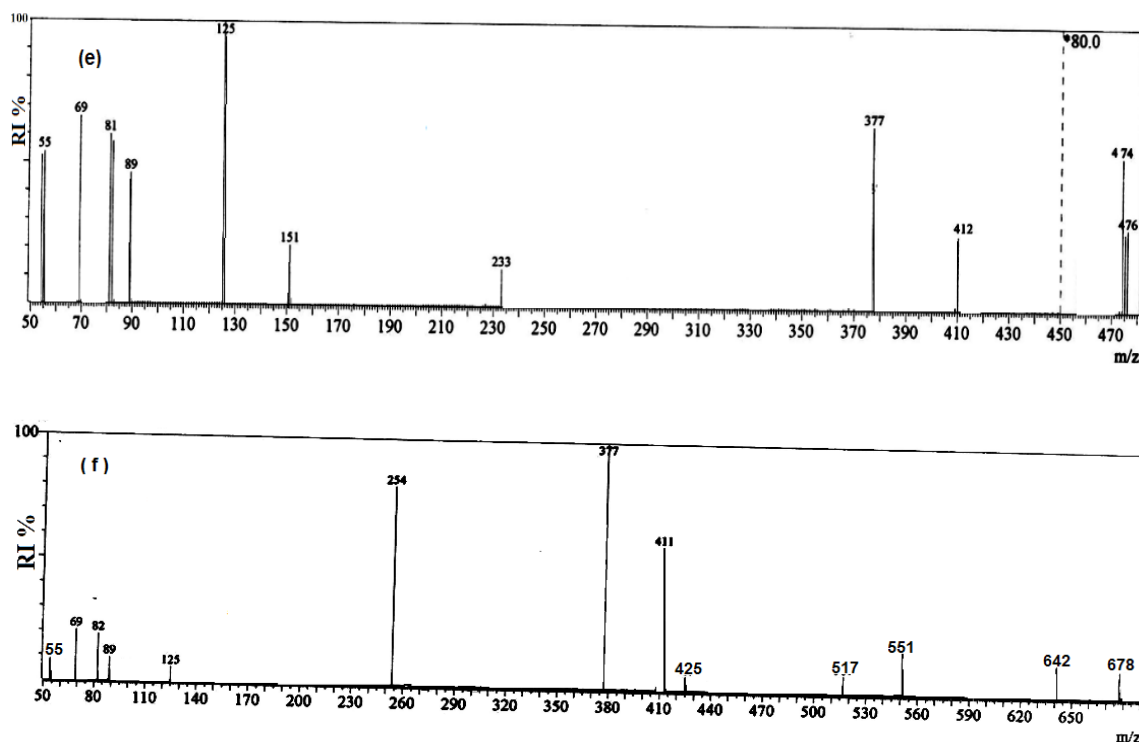


Fig. 12. Mass spectra of (a) VRZ drug (b) VRZ - Rbeng ion-pair (c) FLZ drug (d) FLZ - Rbeng ion-pair (e) BTZ drug (f) BTZ - Rbeng ion-pair.

[30]. All the compounds were tested in vitro for their antibacterial activity against staphylococcus aureus and *Streptococcus mutans* (Gram positive bacteria), *Escherichia coli*, *Pseudomonas aeruginosa* and *klebsiella* (Gram negative bacteria) using nutrient agar medium. Ampicillin and Gentamicin were used as standard drugs for Gram positive and Gram negative respectively. DMSO was used as solvent control. The compounds were tested at a concentration of 15 mg/mL against both bacterial and fungal strains. The results are obtained in Table 2.

From Table 2, it is found that FLZ and VRZ have no antibacterial activity toward *Escherichia coli*, *Klebsiella pneumonia* and *Pseudomonas aeruginosa* in comparison with the standard found in the local market (Gentamicin). It is found that these drugs (FLZ and VRZ) have antibacterial activities after adding RBeng to their structures. FLZ-RBeng and VRZ-RBeng ion-pairs are biologically more active than the parent drugs. In case of BTZ, it is found that it has antibacterial activities toward *Escherichia coli* and *Klebsiella pneumonia* in comparison with the standard found in the local market (Gentamicin). These antibacterial activities toward these two types of bacteria are decreased after adding RBeng

to BTZ structure. BTZ and its ion pair have no antibacterial activities toward *Pseudomonas aeruginosa* in comparison with the standard found in the local market (Gentamicin).

For *Staphylococcus aureus* and *Streptococcus mutans* bacteria, it is found VRZ has antibacterial activity toward *Streptococcus mutans* bacteria, but it has no antibacterial activity toward *Staphylococcus aureus* in comparison with the standard found in the local market (ampicillin). For FLZ, it is found that it has no antibacterial activity toward these two types of bacteria. After adding RBeng to (FLZ and VRZ) structures, the antibacterial activity toward these two types of bacteria had been increased. FLZ-RBeng and VRZ-RBeng ion-pairs are biologically more active than the parent drugs. In case of BTZ, it is found that it has antibacterial activities toward *Staphylococcus aureus* and *Streptococcus mutans* in comparison with the standard found in the local market (Ampicilin). These antibacterial activities toward these two types of bacteria are decreased after adding RBeng to BTZ structure.

For *Candida albicans* fungi, it is found that, FLZ and VRZ have antifungal activity toward this type of fungi in comparison with the standard

TABLE 2. Comparison between the biological activity of standard drugs and their products with Rbeng.

Sample	FLZ	VRZ	BTZ	FLZ-Rbeng	VRZ-Rbeng	BTZ-Rbeng	Standard antibiotic
Microorganism							
Gram negative bacteria							Gentamicin
<i>Escherichia coli</i> (ATCC:3008)	NA	NA	24.7 ± 0.6	24.3 ± 0.6	24.3 ± 1.5	12.7 ± 1.5	35 ± 0.5
<i>Klebsiella pneumonia</i> (ATCC:4415)	NA	NA	27.0 ± 1.7	29.7 ± 3.0	28.3 ± 1.5	17.3 ± 0.6	35 ± 0.5
<i>Pseudomonas aeruginosa</i> (ATCC:27853)	NA	NA	NA	11.7 ± 1.5	14.7 ± 0.6	NA	30 ± 0.5
Gram positive bacteria							Ampicillin
<i>Staphylococcus aureus</i> (ATCC:6538)	NA	NA	19.0 ± 1.0	12.3 ± 1.5	12.0 ± 2.0	13.0 ± 1.0	30 ± 0.1
<i>Streptococcus mutans</i> (ATCC:25175)	NA	19.0 ± 1.0	26.0 ± 1.0	26.3 ± 0.6	29.7 ± 0.6	14.0 ± 1.0	35 ± 0.5
Fungi							Nystatin
<i>Candida albicans</i> (ATCC:10231)	¹⁶ ± 0.5	19.3 ± 0.6	35.3 ± 0.6	33.7 ± 0.6	35.3 ± 0.6	25.7 ± 0.6	20 ± 0.5

- Zone of inhibition is expressed in the form of mean ± standard deviation (mm).
- NA: No activity

found in the local market (Nystatin). After adding RBeng to (FLZ and VRZ) structures, the antifungal activity toward this type of fungi had been increased. In case of BTZ, it is found that it has antifungal activity toward *Candida albicans* fungi in comparison with the standard found in the local market (Nystatin). It is found to be 35.3 ± 0.6 toward *Candida albicans* fungi. This antibacterial activity toward this type of bacteria decreased after adding RBeng to BTZ structure.

It can be concluded that the solid ion-pairs with RBeng are more antibacterial and antifungal agents than their drugs for FLZ and VRZ.

Conclusions

This research successfully concerned with

the preparation, separation and structures elucidation of solid ion-pairs of the selected drugs in reaction with Rbeng.

Comparison between MS and TA helps in selection of the proper pathway representing the decomposition of these drugs.

Comparison between MS and TA of solid Rbeng ion-pairs with their drugs provides further information about chemical behaviours of both drugs and their reaction products also clarify how they react together. From application of both experimental techniques on investigation of solid ion-pairs, it is concluded that the Rbeng anionic form found in entities of these drugs, may effect on their TA and MS fragmentation.

The biological activities of drugs and their Rbeng solid ion-pairs towards five types of bacteria

and one type fungi are studied. It is found that the solid ion-pairs with RBeng are more biological activity than their drugs for FLZ and VRZ, but less biological activity for BTZ than its ion pair.

References

1. Arnold, T. M. Dotson, E., Sarosi G. A. and Hage; C. A. Traditional and emerging antifungal therapies, *Proceedings of the American Thoracic Society*, **7**(3), 222-228 (2010).
2. Georgopapadakou N. H. and Walsh, T. J.; Antifungal agents: Chemotherapeutic targets and immunologic strategies, *Antimicrobial Agents and Chemotherapy*, **40**(2), 279-291(1996).
3. Ghannoum, M. A.; Future of antimycotic therapy, *Dermatologic Therapy*, **3**, 104-111 (1997).
4. Koltin Y. and Hitchcock, C. A.; The search for new triazole antifungal agents, *Current Opinion in Chemical Biology*, **1**(2), 176-182 (1997).
5. White, T. C. , Marr K. A. and Bowden, R. A.; "Clinical, cellular, and molecular factors that contribute to antifungal drug resistance, *Clinical Microbiology Reviews*, **11**(2), 382-402 (1998).
6. Boeira, P., Antunes, M. V., Andreolla, H. F. , Pasqualotto, A. C. and Linden, R.; Ultra-performance liquid chromatographic method for measurement of voriconazole in human plasma and oral fluid, *Journal of the Brazilian Chemical Society*, **23**(1), 148-155 (2012).
7. Jalali, F. and Rajabi; M. J., Extractive spectrophotometric determination of fluconazole by ion-pair complex formation with bromocresol green, *Chinese Journal of Chemistry*, **25**(9), 1300-1303 (2007).
8. United States Pharmacopeia 40th, 2:3089 (2017).
9. Goel, A., Sharma, S., Kaur N. and Sharma, A.; Pharmacokinetic data and solubility profile of antifungal drugs, *International Journal of Pharma Professional's Research*, **2**(2), 256-265 (2011).
10. Basivi, P. K., Pasupuleti, V. R., Seella, R., Tukiakula, M. R., Kalluru, S. R. and Park, S.J.; Inverse gas chromatography study on London dispersive surface free energy and electron acceptor-donor of fluconazole drug, *Journal of Chemical & Engineering Data*, **62**(7), 2090-2094 (2017).
11. Basu, S. S., Petrides, A., Mason, D. S. and Jarolim, P.; A rapid UPLC-MS/MS assay for *Egypt. J. Chem.* **62**, No. 11 (2019)
12. Lei, M. , Yao, H. , Dong, Y., Wang, M. , Wang, Z. and Cheng, X.; Development and validation of an LC-MS/ method for simultaneous quantification of voriconazole and its main metabolite voriconazole n-oxide in human plasma and its clinical application, *Journal of Liquid Chromatography & Related Technologies*, **40**(20), 1047-1053 (2017).
13. Podolska, M., Biał Ecka, W., Kulik, A., Kwiatkowska - Puchniarz B. and Mazurek, A.; HPLC method for separating enantiomers of imidazole derivatives ñ antifungal compounds, *Acta Poloniae Pharmaceutica*, **74**(3), 777-784 (2017).
14. Paul, S., Mohanram K. and Kannan, I.; Antifungal activity, gas chromatographic-mass spectrometric analysis and in silico study of punica granatum peel extracts against fluconazole resistant strains of candida species, *Current Pharmaceutical Biotechnology*, **19**(3), 250-257 (2018).
15. Geballa-Koukoula, A., Panderi, I., Zervas, K., Geballa-Koukoulas, K., Kavvalou, E., Panteri-Petratou, E., Vourna, P. and Gennimata, D.; "A porous graphitized carbon lc-esi/ms method for the quantitation of metronidazole and fluconazole in breast milk and human plasma, *Journal of Chromatography B*, **1084**, 175-184 (2018).
16. Xu, R.-a., Lin, Q., Qiu, X., Chen, J., Shao, Y., Hu, G., and Lin, G.; UPLC-MS/MS method for the simultaneous determination of imatinib, voriconazole and their metabolites concentrations in rat plasma, *Journal of Pharmaceutical and Biomedical Analysis*, **166**, 6-12 (2019).
17. Sasikala, M., Priyanka, P., Kumar, T. V. and Venkateshwarlu, G., Spectrophotometric estimation of drugs using n-bromo succinamide and indigo carmine couple, *Oriental Journal of Chemistry*, **32**(1), 617-625 (2016).
18. Patil, S. S., Ravindra, Tejal, Y., Laxmi, T. Salunke, P., Wagh, R. and Barhate, S.; Comparative study of analytical method development of fluconazole in tablets and capsule by ultraviolet spectrophotometric method, *International Journal of Chemical and Analytical Science*, **7**(1), 1-6 (2017).
19. Anandkumar, Y., Kapse-Mistry, S. and Kadu, P.; UV spectrophotometric method development and the simultaneous measurement of fluconazole, voriconazole, posaconazole, itraconazole, and hydroxyitraconazole concentrations in serum, *Clinical Chemistry and Laboratory Medicine* **55**(6), 836-844 (2017).

- validation for estimation of fluconazole, *World Journal of Pharmaceutical Research*, **4**(11), 814-821 (2015).
20. Reddy, B. V. and Venkateshwarlu, G.; Quantitative determination of drugs and pharmaceuticals using chloramine-t and methyl orange as dye, **7**(12), 658-669 (2018).
21. Codevilla, C. F., Rosa, P., Steppe, M., Bergold, A. M., Rolim, C. M. B. and Adams, A. I. H.; Development and validation of a stability-indicating micellar electrokinetic chromatography method to assay voriconazole tablets, *Analytical Methods*, **5**(19), 5051-5057 (2013).
22. Jebakumar Immanuel Edison, T. and Sethuraman, M.; Electrochemical investigation on adsorption of fluconazole at mild steel/HCL acid interface as corrosion inhibitor, *ISRN Electrochemistry*, **2013**, 1-8 (2012).
23. Lide, D. R.; "CRC Handbook of Chemistry and Physics", 75th edition, Boca Raton, FL: CRC Press, 9-79 (1994).
24. Socrates, G.; "Infrared and Raman Characteristic Group Frequencies: Tables and Charts", John Wiley and Sons, 18 (2004).
25. Silverstein, R. M., Bassler, G. C. and Morrill, T. C.; "Spectrometric Identification of Organic Compounds, 4th edition, New York: Wiley", 166 (1981).
26. Larsen, B. S. and Ewen, C. N. M.; "Mass Spectrometry of Biological Materials", Marcel Dekker, New York (1998).
27. Levsen, k.; "Fundamental Aspects of Organic Mass Spectrometry", Verlag Chemie, Weinheim, New York (1978).
28. Zayed, E. M., Zayed M.A. and El-Desawy, M.; Preparation and structure investigation of novel Schiff bases using spectroscopic, thermal analyses and molecular orbital calculations and studying their biological activities, *Spectrochimica Acta Part A: Molecular and Biomolecular Spectroscopy*, **134**, 155-164 (2015).
29. Zayed, M. A., El-Shal, M. A. and Abdallah, M. A.; Spectrophotometric determination of fluconazole, voriconazole and butoconazole nitrate by ion-pair formation with rose bengal reagent, *Egyptian Journal of Chemistry*, **60**(6), 2077-2088 (2017).
30. Scott, A. C.; "Laboratory control of antimicrobial therapy", In: Collee jg et al. Eds, *Practical Medical Microbiology*, 13th edition, Edinburgh: Churchill livingstone (1989).
31. JM, T., A. K. P and Kulkarni, S. V.; Formulation and evaluation of sustained release matrix tablets of Voriconazole using synthetic polymers, *International Journal for Pharmaceutical Research Scholars*, **4**(2), 24-35(2015).
32. Cyr, T. D., Dawson, B. A, Neville, G. A and Shurvell, H. F.; Spectral characterization of Fluconazole, *Journal of Pharmaceutical and Biomedical Analysis*, **14**, 247-255 (1996).
33. Parashar, B., Kabra, A. and Chandel, A.; Formulation and evaluation of gel containing Miconazole nitrate an antifungal agent, *International Journal of Pharma Research and Review*, **2**(6), 18-28 (2013).
34. Parthibarajan, R., Gowrishankar, N., Rajitha, M., Vinaykumar, A., Himavanthu, M., Ramesh, K. and Vijaya, K.; Formulation and evaluation of Voriconazole floating tablets, *Asian Journal of Pharmaceutical and Clinical Research*, **5**(3), 180-184 (2012).
35. O'Neil, M., Smith, A., Heckelman, P. and Budavari, S.; "Éditeurs. *The Merck Index: An Encyclopedia of Chemicals, Drugs, and Biologicals*", 13 e édition. Whitehouse station (New Jersey): Merck and company, 729 (2001).

دراسة تركيب الأزواج الأيونية الصلبة لثلاثة أدوية مشتقات الأميدازول مع الروزنجال باستخدام تقنيات تحليلية مختلفة ودراسة فعاليتها البيولوجية

محمد زايد¹ و مروه عبدالله²

¹قسم الكيمياء - كلية العلوم - جامعة القاهرة - الجيزة - مصر.

²الهيئة القومية للرقابة والبحوث الدوائية - الجيزة - مصر.

يتعلق العمل الحالي بتحضير وفصل ودراسة التراكيب للأزواج الأيونية الصلبة لثلاث من الادوية مضادة للفطريات الفوريكونازول، الفلوكونازول و البيوتاكونازول نيترات مع الروزنجال. تم خضير الأزواج الأيونية الصلبة وفحصها باستخدام الأشعة تحت الحمراء، التحليل الطيفي للكتلة و التحاليل الحرارية، بالإضافة إلى تقنية التحليل الميكروني للعناصر. تم تحديد الصيغة العامة للأزواج الأيونية. علاوة على ذلك، تم اقتراح صيغ الأزواج الأيونية المعدة وخصيها هيكليا. تمت دراسة الفعالية البيولوجية لهذه الأدوية والأزواج الأيونية المتكونة ضد خمسة انواع من البكتيريا ونوع واحد من الفطريات. بعد مقارنة النتائج وجد أن الأزواج الأيونية للأدوية لها فعالية بيولوجية أعلى من الأدوية نفسها.